

Chandra Observation of Point Sources in the X-Ray Elliptical Galaxy NGC 1407 *

Zhong-Li Zhang^{1,2} and Hai-Guang Xu²

¹ National Astronomical Observatories, Chinese Academy of Sciences, Beijing 100012;
zebrafish@sjtu.edu.cn

² Department of Physics, Shanghai Jiao Tong University, Shanghai 200030; hgxu@sjtu.edu.cn

Received 2003 October 13; accepted 2003 December 18

Abstract With the *Chandra* pointing observation of about 50 ks, we have detected 41 point sources in the X-ray relatively faint elliptical galaxy NGC 1407, most of which appear to be low mass X-ray binaries. In luminosity flux units, these resolved point sources contribute about 17.8% of the total emission of the galaxy in 0.3–10 keV. Of the remaining diffuse emission, about 53.4% (or 43.9% of total) may arise from unresolved point sources. We find six ultraluminous X-ray sources with luminosities above 10^{39} erg s⁻¹. This number is less than has been found in NGC 720, but more than in NGC 4697 and NGC 1553, so suggesting a possible correlation between the number of ULXs and the total X-ray luminosity of early-type galaxies. A central point-like source is detected whose luminosity ($2.36 \pm 0.14 \times 10^{39}$ erg s⁻¹) is the highest among all resolved sources. However, because of its relatively low hardness ratio, we speculate that it is not likely to be a low luminosity AGN.

Key words: binaries: close — galaxies: elliptical and lenticular — galaxies: individual: NGC 1407 — X-rays: binaries — X-rays: galaxies

1 INTRODUCTION

Early X-ray observations of elliptical galaxies with satellites such as *Einstein* and *ROSAT* (c.f. Fabbiano, Kim & Trinchieri 1994) revealed that in the X-ray spectra of these early-type galaxies there is a hard component whose intensity is approximately proportional to the optical luminosity of the galaxy. This hard spectral component has been ascribed to a population of low-mass X-ray binaries (LMXBs). In X-ray bright elliptical galaxies, whose X-ray to optical luminosity ratio L_X/L_B is relatively high, the hard component is usually dominated by a softer thermal component emitted by the interstellar medium (ISM); in X-ray faint elliptical galaxies, the hard component dominates over the total X-ray emission of the galaxy. Therefore, X-ray faint elliptical galaxies are ideal sites for studying the X-ray property of the LMXB population. However, before the superb spatial resolution of the *Chandra* X-ray Observatory became available, little was known about LMXB in X-ray faint elliptical galaxies.

* Supported by the National Natural Science Foundation of China.

In 2000 and 2001, with a 39.4 ks *Chandra* pointing observation, Sarazin, Irwin & Bregman found that in the X-ray faint elliptical galaxy NGC 4697 more than half of the observed X-ray counts from within one effective radius can be resolved into ~ 80 LMXBs. If we take into account the contribution of those unresolved fainter LMXBs, then about 77% of the total counts may arise from LMXBs. This ratio is higher than that found in the X-ray faint S0 galaxy NGC 1553 as reported in Blanton, Sarazin & Irwin (2001). Among the ~ 80 resolved point sources in NGC 4697, there are three super soft sources (SSSs) with no detectable emission beyond 1 keV. Since the distances of the three SSSs to the galactic center are small, they are considered to belong to the galaxy. In NGC 1553 and another elliptical galaxy NGC 720 (Jeltema et al. 2003), however, no such soft sources were found. The X-ray luminosity in 0.3–10 keV of all the detected point sources in NGC 720, NGC 1553, and NGC 4697 have been calculated by the authors. After normalizing the obtained luminosities Hubble constant $H_0 = 75 \text{ km s}^{-1} \text{ Mpc}^{-1}$, there are seven ultraluminous X-ray sources (ULXs; sources with their luminosities exceeding $10^{39} \text{ erg s}^{-1}$) in NGC 720, three in NGC 1553, and one in NGC 4697. These ultraluminous X-ray sources may be associated with accreting black holes of intermediate masses, or with beamed emission from ordinary black hole and/or neutron star binaries. As of today, SSSs and ULXs have been found in a variety of galaxies (e.g., Holt et al. 2003; Mukai et al. 2003; Pence et al. 2001). However, their physical nature and the reason why their occurrence varies so much in different types of galaxies are still under investigation.

In this paper, we present some preliminary results of a *Chandra* study of the point sources in the elliptical galaxy NGC 1407. Sitting at the center of the Eridanus A cluster, NGC 1407 is one of the nearest X-ray relatively faint elliptical galaxies with a redshift of 0.0059, which makes it an ideal target for the study of LMXB population in early type galaxies. By analyzing the *ROSAT* PSPC pointing observations, O’Sullivan, Forbes & Ponman (2001) found that the X-ray-to-optical luminosity ratio of NGC 1407 is $L_X(0.3\text{--}10 \text{ keV})/L_B = 2.63 \times 10^{30} \text{ erg s}^{-1} L_{B\odot}^{-1}$. Optical study of NGC 1407 (Gould 1993; Perrett et al. 1997; Quintana, Fouque & Way 1994) revealed that its mass-to-light ratio is extremely large, which means that it may be a highly dark-matter-dominated system possibly containing a large population of LMXBs.

We describe the observation and data reduction in Sect. 2. In Sect. 3, we present the *Chandra* image and compare it with the optical results. Then in Sect. 4, we investigate the X-ray properties of the resolved point sources by studying their hardness ratios. After sorting the point sources into five groups, we make direct spectral fittings of the integrated spectrum of each group. In Sect. 5, we summarize and discuss the implications of our results by comparing them with those obtained for NGC 720, NGC 4697 and NGC 1553. The distance to NGC 1407 has been measured with a variety of methods. Unless stated otherwise, throughout this paper we adopt a distance of 20.61 Mpc (O’Sullivan, Forbes & Ponman 2001), assuming a Hubble constant of $75 \text{ km s}^{-1} \text{ Mpc}^{-1}$. The solar abundance ratios are taken from Anders & Grevesse (1989), and the errors of the model parameters at 90% confidence are calculated.

2 OBSERVATIONS AND DATA REDUCTION

NGC 1407 was observed with the *Chandra* Advanced CCD Imaging Spectrometer (ACIS) on August 26, 2000 for a total exposure of 50 339 s. The data were telemetered in Faint mode with a frame time of 3.2 s, and the CCD temperature was $-110 \text{ }^\circ\text{C}$. The center of the galaxy was positioned on the ACIS-S3 CCD, with an offset of $0.63'$ from the nominal pointing for the S3 chip. In addition to it ACIS CCDs I2–3, S1–2 and S4 were also in operation. In this paper,

we utilize the data from the S3 chip only, which includes the entire galaxy. We processed the data with the standard *Chandra* analysis package CIAO (version 2.3). After eliminating time intervals of bad aspect and high background, the resulted clean exposure time was 48 475 s. Bad pixels and bad columns have been removed. Only those events with ASCA grades 0, 2, 3, 4 and 6, and with photon energies in the range of 0.3–10 keV were included in our analysis.

3 X-RAY IMAGE

We extracted the *Chandra* S3 image of NGC 1407 in 0.3–10.0 keV and smoothed it to a minimum signal-to-noise ratio of 3σ . The result is shown in Fig. 1, where the image has been corrected for exposure and is plotted on logarithmic scale. It can be seen that the spatial distributions of both the diffuse X-ray emission of ISM and X-ray point sources are roughly symmetric. The X-ray peak of the galaxy is found at RA=03^h40^m11.8^s DEC=−18°34′ 48.3″ (J2000). We notice that this position coincides with the optical center to within 0.3″, less than the uncertainty caused by the aspect offset. In Fig. 2, we overlay the X-ray intensity contours on the optical image of the same region as shown in Fig. 1. To show the spatial distribution of the resolved X-ray point sources, we mark their positions with circles. We found no apparent optical counterpart to any of the resolved X-ray point sources.

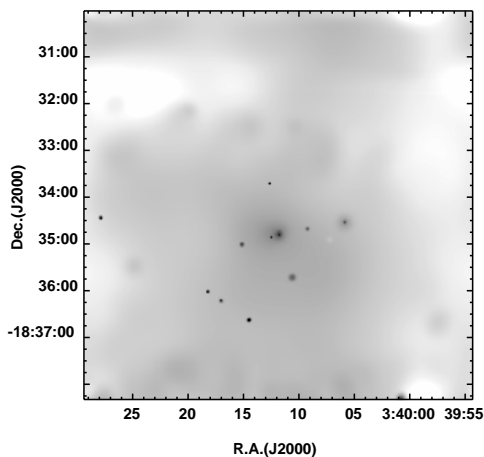


Fig. 1 Smoothed image of the central region of NGC 1407. The image has been corrected for exposure and is plotted in logarithmic scale.

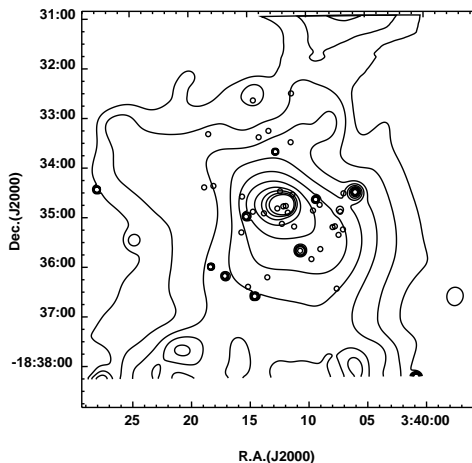


Fig. 2 DSS optical image of NGC 1407, on which positions of the resolved X-ray sources and X-ray intensity contours are overlaid. Contours are spaced from $9 \times 10^{-10} \text{ ph cm}^{-2} \text{ s}^{-1} \text{ pix}^{-2}$ to $1.5 \times 10^{-9} \text{ ph cm}^{-2} \text{ s}^{-1} \text{ pix}^{-2}$ in logarithmic scale.

4 POINT SOURCES

We identified the X-ray point sources by using a sliding cell detection algorithm. The detection threshold was set to be 3σ . We also used a wavelet-based detection algorithm and eye-examination to cross-check the result. Within two effective radii of NGC 1407 (1 effective radius = 1.17′, Matsushita 2001), we detected a total of 41 point sources. The count rates of

these point sources were corrected for both exposure and background. The background was determined for each point source from its surrounding regions.

4.1 Hardness Ratio

Since the total count of each point source is low, simple model fits to the X-ray spectrum of an individual source will not yield unambiguous determinations. So we first investigate the hardness ratios of those resolved point sources, for which we are able to obtain spectral information to some extent. Following other works (e.g., Sarazin, Irwin & Bregman 2000, 2001), we divided the entire energy band into three parts (i.e., soft S: 0.3–1 keV, medium M: 1–2 keV, and hard H: 2–10 keV), and then calculated the hardness ratios $H21=(M-S)/(M+S)$ and $H31=(H-S)/(H+S)$. The results are plotted in Fig. 3 as a color-color diagram. In this figure, the upper solid line represents the predicted ratios for a power-law model with a hydrogen column density equal to the Galactic value ($5.42 \times 10^{20} \text{ cm}^{-2}$, Dickey & Lockman 1990). From top to bottom, the filled squares on this line mark the photon indices of 0.0, 0.5, 1.0, 1.5, 2.0, 2.5, 3.0, 3.5 and 4.0. The lower line is the same as the upper one except that the hydrogen column density is set to be 5 times the Galactic value and the photon indices from 1.0 to 6.0. Error bars are quoted based on a binomial distribution of the source counts in each band.

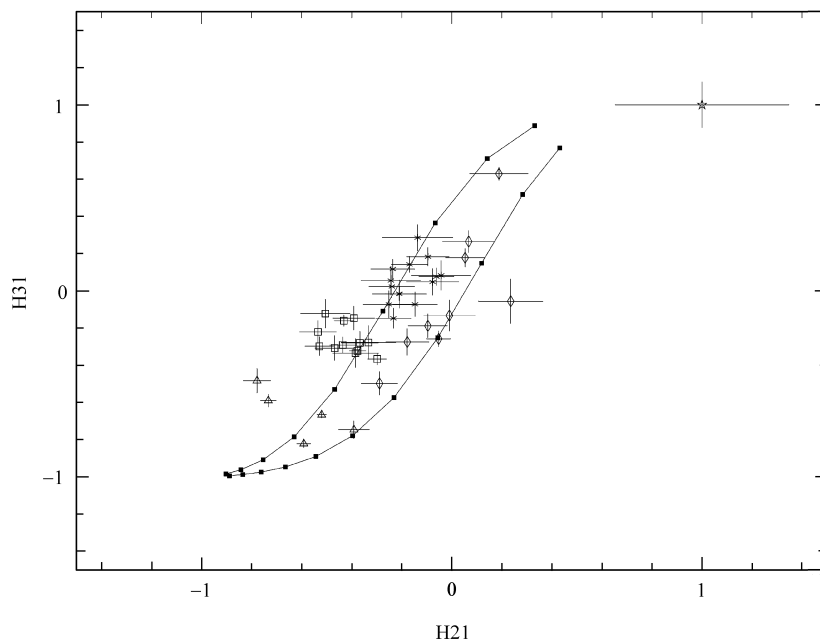


Fig. 3 Color-color diagram of the resolved point sources. The hardness ratios are defined as $H21=(M-S)/(M+S)$ and $H31=(H-S)/(H+S)$, where S, M, and H represent the corrected counts in 0.3–1 keV, 1–2 keV, and 2–10 keV. The upper line shows the predicted ratios for a power-law spectral model with its absorption equal to the Galactic value. From top to bottom, the full square marks on the line are for photon indices of 0.0, 0.5, 1.0, 1.5, 2.0, 2.5, 3.0, 3.5 and 4.0. The lower line is the same as the upper one except that the absorption is 5 times the Galactic value and the photon indices from 1.0 to 6.0. Point sources of five different groups are represented with different marks.

According to their locations on the color-color diagram, we sort the sources into five groups as shown with different marks (see also Table 1). Group 1 includes five softest sources marked with triangles; they are not so soft as SSSs, though. The photon indices Γ_{ph} of these soft sources range from 1.5 to 3.0. Sources in group 2 (crosses) and group 3 (open squares) are located quite close to the upper line, while sources in group 2 have photon indices of 1.0–1.5, and sources in group 3 have relatively larger indices (1.5–2.0). Sources in group 4 (diamonds) are located close to the lower line. They are most likely to be background sources. There is only one source in group 5 (star), which is the hardest one ($H21=1.0 \pm 0.347$, $H31=1.0 \pm 0.124$) among the 41 resolved sources. This source is located far ($1.9'$) from the galactic center, so that it may be an unrelated, strongly absorbed background AGN.

Table 1 41 Detected X-ray Point Sources in NGC 1407

Source	R.A. (J2000)	Dec. (J2000)	d^{*1} (arcsec)	Count *2	Luminosity (0.3–10 keV) ($10^{38} h_{75}^{-2} \text{ erg s}^{-1}$)	SNR (σ)	group
1	03 : 40 : 11.790	-18 : 34 : 48.96	0.3	364.4 ± 21.0	23.59 ± 1.36	5.48	1
2	03 : 40 : 12.003	-18 : 34 : 49.38	2.8	45.9 ± 10.3	3.25 ± 0.73	0.94	1
3	03 : 40 : 11.631	-18 : 34 : 56.91	8.3	131.6 ± 12.3	9.39 ± 0.88	7.71	1
4	03 : 40 : 12.512	-18 : 34 : 51.75	10.4	127.9 ± 12.1	12.00 ± 1.14	8.29	2
5	03 : 40 : 11.220	-18 : 34 : 35.18	16.3	64.2 ± 8.6	4.55 ± 0.61	8.16	2
6	03 : 40 : 12.264	-18 : 34 : 31.10	19.2	32.5 ± 6.5	2.40 ± 0.48	4.20	2
7	03 : 40 : 12.140	-18 : 35 : 10.44	22.0	20.3 ± 5.9	1.50 ± 0.44	2.30	2
8	03 : 40 : 11.095	-18 : 35 : 13.91	27.0	24.8 ± 5.7	2.33 ± 0.54	4.45	2
9	03 : 40 : 13.656	-18 : 34 : 57.55	27.8	28.1 ± 6.0	2.60 ± 0.55	4.67	4
10	03 : 40 : 09.477	-18 : 34 : 54.77	33.8	39.6 ± 7.1	6.00 ± 1.07	5.84	1
11	03 : 40 : 09.249	-18 : 34 : 41.54	37.4	57.6 ± 7.9	6.20 ± 0.85	16.48	3
12	03 : 40 : 14.600	-18 : 34 : 55.39	40.4	36.5 ± 6.4	3.22 ± 0.56	13.86	4
13	03 : 40 : 08.914	-18 : 34 : 47.94	41.4	100.4 ± 10.3	12.08 ± 1.24	22.14	4
14	03 : 40 : 15.175	-18 : 35 : 01.35	49.7	30.0 ± 5.9	2.56 ± 0.50	13.67	3
15	03 : 40 : 15.507	-18 : 34 : 37.13	54.2	22.0 ± 5.1	2.14 ± 0.50	8.52	3
16	03 : 40 : 10.611	-18 : 35 : 43.25	57.1	91.6 ± 9.8	9.42 ± 1.00	61.00	3
17	03 : 40 : 07.834	-18 : 35 : 15.00	62.6	50.0 ± 7.3	4.40 ± 0.64	22.53	3
18	03 : 40 : 15.593	-18 : 35 : 20.38	62.6	18.4 ± 4.7	2.34 ± 0.60	8.60	3
19	03 : 40 : 07.634	-18 : 35 : 14.08	64.8	29.1 ± 5.7	2.48 ± 0.49	26.56	2
20	03 : 40 : 07.169	-18 : 34 : 56.49	66.8	44.8 ± 7.0	3.82 ± 0.60	15.00	2
21	03 : 40 : 08.889	-18 : 35 : 41.37	67.2	28.2 ± 5.6	3.42 ± 0.68	23.00	4
22	03 : 40 : 12.636	-18 : 33 : 43.24	67.3	31.7 ± 5.9	5.05 ± 0.93	19.31	4
23	03 : 40 : 09.654	-18 : 35 : 53.46	71.7	18.2 ± 4.9	1.89 ± 0.50	5.46	2
24	03 : 40 : 06.874	-18 : 34 : 34.24	72.2	29.1 ± 5.6	3.44 ± 0.67	19.80	4
25	03 : 40 : 07.330	-18 : 35 : 24.52	73.3	19.7 ± 4.8	1.59 ± 0.39	11.00	2
26	03 : 40 : 06.948	-18 : 35 : 17.96	75.4	22.9 ± 5.1	2.36 ± 0.53	12.14	3
27	03 : 40 : 11.334	-18 : 33 : 31.82	78.0	44.6 ± 6.8	6.78 ± 1.03	57.67	3
28	03 : 40 : 05.888	-18 : 34 : 32.90	86.2	59.1 ± 8.0	7.13 ± 0.96	23.00	3
29	03 : 40 : 13.424	-18 : 36 : 14.97	89.4	51.4 ± 7.5	6.52 ± 0.95	18.43	4
30	03 : 40 : 14.045	-18 : 33 : 25.43	90.0	15.2 ± 4.1	2.57 ± 0.70	29.00	4
31	03 : 40 : 17.930	-18 : 34 : 23.88	91.2	20.0 ± 4.8	2.22 ± 0.53	15.00	3
32	03 : 40 : 13.210	-18 : 33 : 17.87	93.9	36.4 ± 6.3	3.41 ± 0.59	42.43	3
33	03 : 40 : 18.718	-18 : 34 : 25.43	101.7	22.7 ± 5.0	2.13 ± 0.50	21.86	3
34	03 : 40 : 15.069	-18 : 36 : 26.18	108.2	17.7 ± 4.7	1.91 ± 0.51	12.14	3
35	03 : 40 : 17.040	-18 : 36 : 12.88	112.7	25.9 ± 5.6	13.00 ± 2.83	13.93	5
36	03 : 40 : 14.509	-18 : 36 : 37.88	116.1	168.3 ± 13.2	13.57 ± 1.06	58.13	2
37	03 : 40 : 18.267	-18 : 36 : 01.84	117.8	151.6 ± 12.5	12.37 ± 1.01	100.33	2
38	03 : 40 : 07.522	-18 : 36 : 29.55	118.2	22.2 ± 5.6	1.68 ± 0.42	6.70	2
39	03 : 40 : 18.331	-18 : 33 : 21.06	128.6	31.6 ± 5.9	3.00 ± 0.56	36.71	3
40	03 : 40 : 14.504	-18 : 32 : 40.85	134.7	38.9 ± 6.5	4.14 ± 0.69	41.00	4
41	03 : 40 : 11.263	-18 : 32 : 32.77	137.4	17.7 ± 4.4	1.51 ± 0.37	75.00	1

*1 Radial distance to the center of the galaxy. *2 Count corrected for exposure and background.

Based on the calculated hardness ratios H21 and H31, we estimated the absorption-corrected luminosities of all the resolved point sources, assuming they are located at the distance of NGC 1407. The obtained 0.3–10 keV X-ray luminosities (Table 1) range from $1.50 \pm 0.44 \times 10^{38}$ erg s $^{-1}$ to $2.36 \pm 0.14 \times 10^{39}$ erg s $^{-1}$, this indicates that most point sources have their origins as accreting neutron stars in LMXB systems. There are six ultraluminous sources with luminosities exceed 10^{39} erg s $^{-1}$. The central source has the highest luminosity of $2.36 \pm 0.14 \times 10^{39}$ erg s $^{-1}$.

4.2 Spectral Fitting

After subtracting all the resolved point sources, we have extracted the radial surface brightness profile of NGC 1407 in 0.7–7 keV to determine the boundary of X-ray emitting gas (R_{out}), defined as the radius where the count rate is 3 times of background fluctuation higher than the background. The obtained R_{out} is $2.46'$, or 14.75 kpc, which is approximately 2 times the effective radius of NGC 1407. Within this radius, we have extracted the spectrum of the total emission of the galaxy (ISM + all point sources) and, by excluding the resolved sources, the spectrum of the diffuse emission component (ISM + unresolved point sources). The extractions are limited in 0.7–7 keV to avoid uncertainties in the spectral calibrations at the lower energies and to reduce the effect of background at the higher energies. Results of detailed spectral fitting to these spectra are summarized in Table 2 and will be discussed below. In the fitting, we fixed the absorption at the Galactic value, for the fitting was not improved significantly when we allowed it to vary freely. The background spectra were extracted from regions outside R_{out} on the S3 chip.

Table 2 Best-fit Spectral Models for the Total Emission, Diffuse Emission and Resolved Point Sources

Spectral Component*	kT_X (keV)	Abundance (solar)	Γ_{ph}	Luminosity (0.3–10 keV) ($10^{40} h_{75}^{-2}$ erg s $^{-1}$)	$\chi^2/\text{d.o.f.}$
Total Emission (apec+powerlaw)					
apec	$0.79^{+0.01}_{-0.02}$	$0.40^{+4.60}_{-0.11}$	–	4.02	1.49
powerlaw	–	–	$1.56^{+0.17}_{-0.28}$	6.48	
Diffuse Emission (apec+powerlaw)					
apec	$0.79^{+0.01}_{-0.02}$	$0.40^{+4.6}_{-0.16}$	–	3.94	1.55
powerlaw	–	–	$1.59^{+0.23}_{-0.42}$	4.52	
Resolved Sources (powerlaw)					
powerlaw	–	–	$1.38^{+0.12}_{-0.11}$	1.52	1.22

* N_{H} is fixed at the Galactic value 0.0542×10^{20} cm $^{-2}$, and the redshift is set to be 0.005934.

We first fit the spectrum of the total emission with a model including an apec (<http://he-www.harvard.edu.cn/APEC>) spectral component and a power-law spectral component, that are photoelectrically absorbed (Fig. 4 and Table 2). Here, the apec and power-law components are used to represent the emissions from ISM and all (resolved and unresolved) point sources, respectively. The obtained best-fit temperature of the apec component is $\sim 0.786^{+0.011}_{-0.012}$ keV, if the abundance is fixed at ~ 0.4 solar, and the best-fit photon index is $1.56^{+0.17}_{-0.28}$. With the best-fit model, we find that the total flux of the galaxy in 0.3–10 keV is $2.07 \pm 0.09 \times 10^{-12}$ erg cm $^{-2}$ s $^{-1}$, in which the power-law component contributes $1.28 \pm 0.11 \times 10^{-12}$ erg cm $^{-2}$ s $^{-1}$ or $61.7^{+8.5\%}_{-7.5\%}$.

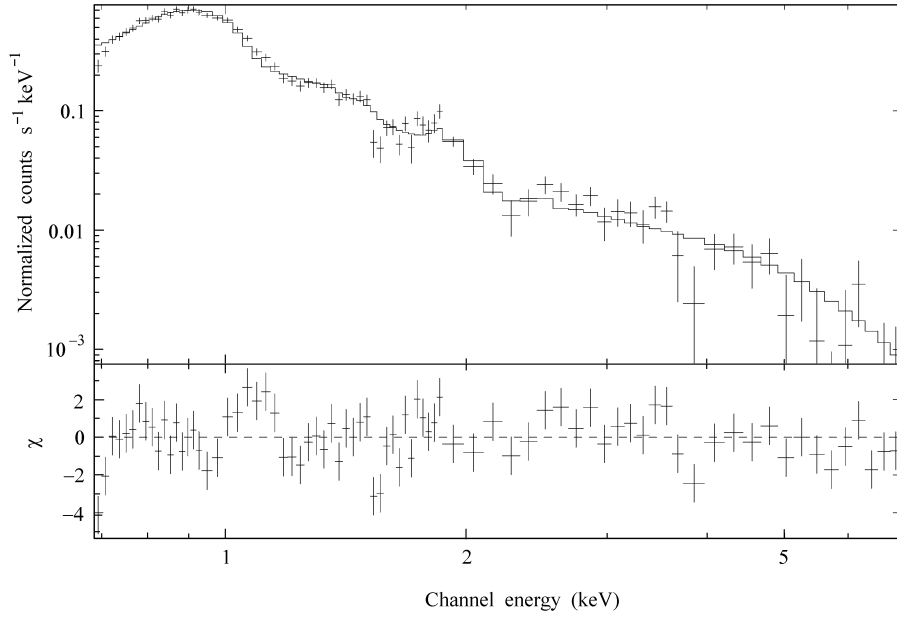


Fig. 4 Observed X-ray spectrum of the total emission within 2.46' from the center and its best-fit model.

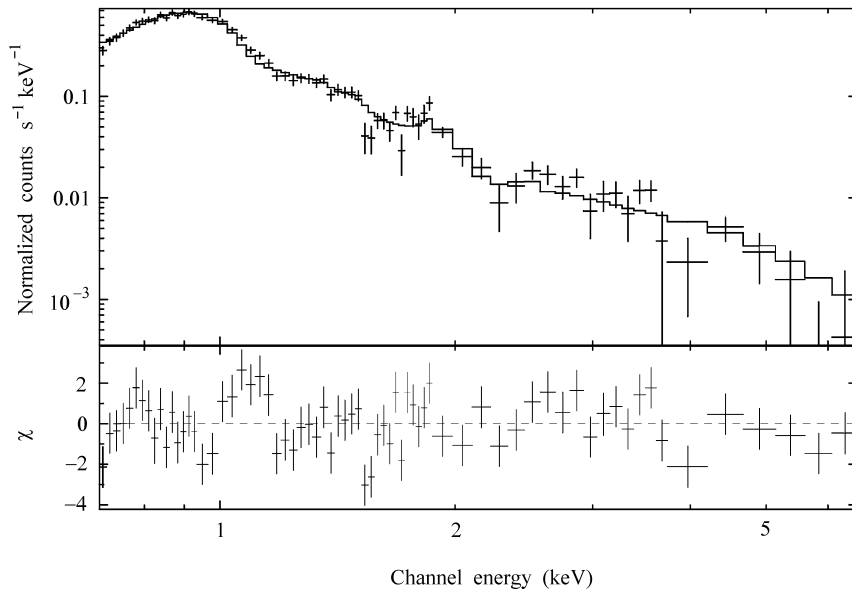


Fig. 5 Observed X-ray spectrum of the diffuse emission within 2.46' from the center and its best-fit model.

Next, by excluding all the resolved point sources, we extract and fit the spectrum of the diffuse emission component (Fig. 5 and Table 2). We use the same spectral model as described above for the total emission, in which the apec component represents the emission from the ISM while the power-law component represents the emission from the unresolved point sources. We find that, with the abundance fixed at 0.4 solar, the best-fit temperature of the thermal component and the best-fit photon index are $\sim 0.786_{-0.016}^{+0.015}$ keV and $\sim 1.59_{-0.42}^{+0.23}$, respectively. These results agree very well with those for the total emission at the 90% confidence level. The 0.3–10 keV flux of the diffuse emission is $1.67 \pm 0.08 \times 10^{-12}$ erg cm $^{-2}$ s $^{-1}$, to which the non-thermal component (unresolved point sources) contributes $8.90 \pm 0.99 \times 10^{-13}$ erg cm $^{-2}$ s $^{-1}$. Thus, it is likely that about half of the diffuse emission is from point sources that are too faint to be resolved with *Chandra*. The rest ($7.80 \pm 1.27 \times 10^{-13}$ erg cm $^{-2}$ s $^{-1}$) should have its origin as the emission from ISM. This value agrees very well with the result derived in the fittings of the total emission.

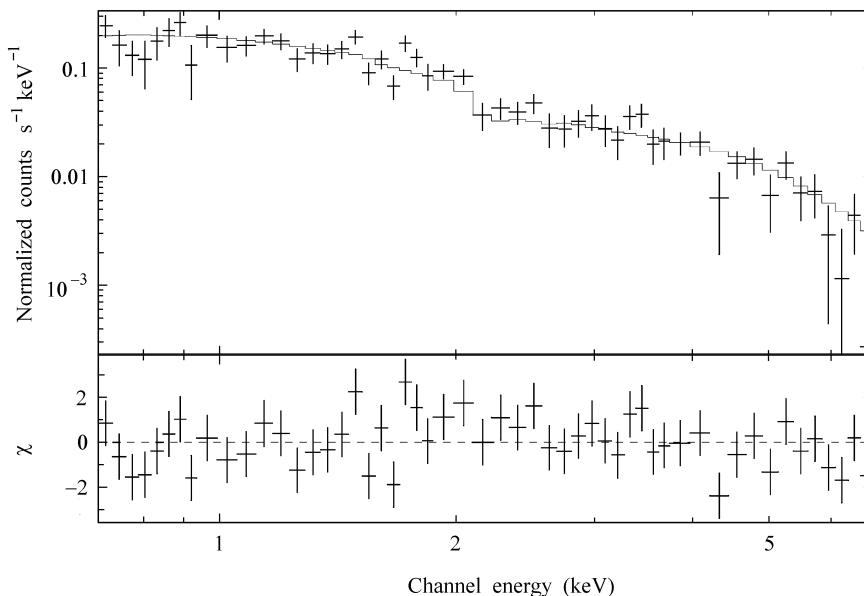


Fig. 6 Observed X-ray spectrum of the resolved sources and its best-fit model.

Finally, we fit the accumulated spectrum of all resolved X-ray point sources (Fig. 6 and Table 2). In order to avoid any possible bias, we exclude the central source whose X-ray luminosity is the highest. We find that the spectrum can be well fitted with a single power-law model, if the absorption is fixed at Galactic value. The derived best-fit photon index is $\sim 1.38_{-0.11}^{+0.12}$, which is again consistent with the values that we have found for the non-thermal component as presented above. The net flux of the resolved point sources is $3.00 \pm 0.21 \times 10^{-13}$ erg cm $^{-2}$ s $^{-1}$.

5 CONCLUSIONS

Within about two effective radii of the X-ray relatively faint elliptical galaxy NGC 1407, we have resolved 41 X-ray point sources with the *Chandra* ACIS instrument. On comparing the

X-ray image with the optical image of the same region, we did not find any apparent optical counterpart of these X-ray point sources.

Using the exposure and background corrected counts in 0.3–1 keV, 1–2 keV and 2–10 keV, we have calculated the hardness ratios of all resolved sources and presented the results in a color-color diagram. There is one very hard source whose hardness ratios are $H_{21}=1.0 \pm 0.347$ and $H_{31}=1.0 \pm 0.124$, possibly indicating a large absorption. We speculate that it is most likely a background AGN. Similar hard sources have been found in two other elliptical galaxies, NGC 720 (Jeltema et al. 2003) and NGC 4697 (Sarazin, Irwin & Bregman 2000, 2001). There are five relatively soft sources in NGC 1407, including the source at the galactic center with a luminosity of $2.36 \pm 0.14 \times 10^{39}$ erg s⁻¹. Unlike the central point sources found in NGC 720, NGC 4697 and NGC 1553, the central source in NGC 1407 may not be an AGN, because it significantly lacks hard X-ray emission; its 2–10 keV flux is $< 7.2 \times 10^{-5}$ erg s⁻¹, contributing $< 30\%$ to its total emission in 0.3–10 keV. No super soft sources with $H_{21} \sim -1$ and $H_{31} \sim -1$ were found in NGC 1407.

Assuming a Hubble constant of 75 km s⁻¹ Mpc⁻¹, we find that the calculated 0.3–10 keV luminosities of the 41 resolved point sources range from $1.50 \pm 0.44 \times 10^{38}$ erg s⁻¹ to $2.36 \pm 0.14 \times 10^{39}$ erg s⁻¹. This indicates that most of the point sources are LMXBs. We also find there are six ultraluminous X-ray sources in NGC 1407 whose X-ray luminosity exceeds 10^{39} erg s⁻¹. This number (N_{ULX}) is about the same as for NGC 720 (*seven*, Jeltema et al. 2003), and is more than for NGC 1553 (*three*, Blanton, Sarazin & Irwin 2001) and NGC 4697 (*one*, Sarazin, Irwin & Bregman 2000, 2001). We notice that there seems to be a correlation between N_{ULX} and the total X-ray luminosity L_X of the early type galaxies (Table 3). To validate this, further study of a larger sample is needed.

Table 3 A Brief Comparison between Four Early-type Galaxies*¹

Name	Distance* ² Mpc	L_X * ³ (10^{40} erg s ⁻¹)	L_B ($10^{10} L_{B\odot}$)	L_X/L_B (10^{30} erg s ⁻¹ $L_{B\odot}^{-1}$)	L'_X * ⁴ (10^{40} erg s ⁻¹)	L'_X/L_X	n_{ps} * ⁵	n_{ULX} * ⁶
NGC 1407	20.61	10.0	3.80	2.63	6.17	0.617	41	6
NGC 4697	15.14	1.32	3.55	0.37	0.94	0.713	80	1
NGC 1553	14.45	3.31	4.27	0.75	1.79	0.540	49	3
NGC 720	20.80	4.07	2.40	1.70			42	7

*¹ Except for the distance, data for NGC 720, NGC 1553, and NGC 4697 are quoted from Jeltema et al. (2003), Blanton, Sarazin, and Irwin (2001), and Sarazin, Irwin, and Bregman (2000, 2001).

*² Distances to these galaxies are quoted from O'Sullivan, Forbes and Ponman (2001) assuming $H_0 = 75$ km s⁻¹ Mpc⁻¹.

*³ Total X-ray luminosity in 0.3–10 keV.

*⁴ X-ray luminosity of all (resolved + unresolved) point sources in 0.3–10 keV.

*⁵ Number of resolved point sources.

*⁶ Number of detected ULXs.

From the spectral model fittings we find that the resolved point sources contribute about 17.8% of the total emission of the galaxy in 0.3–10 keV. Of the remaining diffuse emission, about 53.4% (or 43.9% of total) may arise from the unresolved point sources. Thus, LMXBs may contribute up to 61.7% of the total X-ray flux of NGC 1407. This ratio is higher than in NGC 1553 (54%; Blanton, Sarazin & Irwin 2001), but lower than in NGC 4697 (71.3%; Sarazin, Irwin & Bregman 2000, 2001).

Acknowledgements This work was supported by the National Natural Science Foundation of China (Grant Nos. 10273009 and 10233040) and the Ministry of Science and Technology of China (No. NKBRSF G19990754).

References

- Anders E., Grevesse N., 1989, *Geochimicaet Cosmochimica Acta*, 53, 197
- Blanton E. L., Sarazin C. L., Irwin J. A., 2001, *ApJ*, 552, 106
- Dickey J. M., Lockman F. J., 1990, *ARA&A*, 28, 215
- Fabbiano G., Kim D. -W., Trinchieri G., 1994, *ApJ*, 429, 94
- Gould A., 1993, *ApJ*, 403, 37
- Holt S. S., Schlegel E. M., Hwang U., Petre R., 2003, *ApJ*, 588, 792
- Jeltema T. E., Canizares C. R., Buote D. A., Garmire G. P., 2003, *ApJ*, 585, 756
- Matsushita K., 2001, *ApJ*, 547, 693
- Mukai K., Pence W. D., Snowden S. L., Kuntz K. D., 2003, *ApJ*, 582, 184
- O'Sullivan E., Forbes D. A., Ponman T. J., 2001, *MNRAS*, 328, 4610
- Pence W. D., Snowden S. L., Mukai K., Kuntz K. D., 2001, *ApJ*, 561, 189
- Perrett K. M., Hanes D. A., Butterworth S. T., Kavelaars J., Geisler D., Harris W. E., 1997, *AJ*, 113, 895
- Quintana H., Fouque P., Way M. J., 1994, *A&A*, 283, 722
- Sarazin C. L., Irwin J. A., Bregman J. N., 2000, *ApJ*, 554, L101
- Sarazin C. L., Irwin J. A., Bregman J. N., 2001, *ApJ*, 556, 533